Mechanistic Study of Hydrothermal Management in Air Cooled PEMFCs by Coordinated Ultrasonic Atomization and Fan Regulation Through Three Dimensional Multiphysics Coupling

Jing Qin *, Haoran Ma , Xing Huang , Haotian Yang

Posted Date: 8 April 2026

doi: 10.20944/preprints202604.0542.v1

Keywords: air-cooled PEMFCs; hydrothermal management; ultrasonic atomization; fan speed regulation; evaporation phase change

 doi:10.20944/preprints202604.0542.v1

Article

Mechanistic Study of Hydrothermal Management in Air Cooled PEMFCs by Coordinated Ultrasonic Atomization and Fan Regulation Through Three Dimensional Multiphysics Coupling

Jing Qin [1,2,*], Haoran Ma [1,2], Xing Huang [1,2] and Haotian Yang [1]

[1] College of Automotive and Energy Engineering, Tongji University, Shanghai 201804, China

[2] National Fuel Cell Vehicle and Powertrain System Engineering Research Center, Tongji University, Shanghai 201804, China

* Correspondence: qinjing@tongji.edu.cn

Abstract

To address the difficulty of simultaneously achieving effective heat dissipation and adequate humidification in open cathode air cooled proton exchange membrane fuel cells (PEMFCs) under medium and high power operation, this study proposes a hydrothermal management strategy based on coordinated ultrasonic atomization humidification and fan speed regulation. A three dimensional single cell multiphysics model is developed and validated using a 300 W experimental platform. The effects of atomization frequency and water temperature on stack performance and internal hydrothermal distribution are systematically investigated. Results show that ultrasonic atomization provides inlet precooling, latent heat absorption, and active region humidification, thereby improving hydrothermal uniformity within the stack. Under the optimal condition of 100 kHz and 55 °C, the peak stack power increases by 21.0% to 319.00 W, while voltage consistency and surface temperature uniformity are also improved. Analysis based on the Stokes number and Dalton's law of partial pressures indicates that the optimum results from a balance between suppressing droplet agglomeration and inertial deposition, and limiting oxygen dilution caused by excessive water vapor. The proposed strategy provides a compact and practical approach for improving the stability, uniformity, and efficiency of air cooled PEMFCs.

Keywords: air-cooled PEMFCs; hydrothermal management; ultrasonic atomization; fan speed regulation; evaporation phase change

1. Introduction

Under the dual pressures of the energy crisis and environmental pollution, hydrogen energy has become a strategic priority in the global transition toward green energy owing to its advantages of zero emissions, renewability, and high energy density [1]. Proton exchange membrane fuel cells (PEMFCs) offer high energy conversion efficiency, low operating temperature, rapid start-up, and environmental friendliness, and are therefore regarded as one of the most promising electrochemical energy devices in the fields of transportation, portable power sources, and distributed energy systems [2,3]. Compared with conventional liquid-cooled systems, open-cathode air-cooled PEMFCs eliminate the need for an independent cooling loop, circulation pump, and related auxiliary components, thereby offering advantages such as compact structure, light weight, low parasitic power consumption, and high system integration, which has led to widespread attention in unmanned aerial vehicles, portable power sources, and low-power mobile energy systems [4,5].

However, the output performance and durability of PEMFCs depend strongly on the multiphysics coupling behavior within the membrane electrode, particularly the coupled transport

 doi:10.20944/preprints202604.0542.v1

of heat, water, and reactant gases through the membrane, catalyst layer, gas diffusion layer, and flow channels [6,7]. The proton conductivity of PEMFCs depends strongly on the water content of the perfluorosulfonic acid (PFSA) membrane, and under high power operation, sufficient membrane humidification must be maintained to ensure high ionic conductivity. At the same time, intense electrochemical reactions under high load operation generate a large amount of heat. Studies have shown that when the core temperature of the stack exceeds 80 °C, the mechanical strength of the proton exchange membrane decreases significantly, while the thermal dissociation of sulfonic acid groups within the membrane accelerates, leading to irreversible damage to the membrane electrode assembly (MEA) [1]. Thus, enhancing convective heat transfer through cooling fans is crucial for removing excess heat. However, under air-cooled PEMFC conditions, increasing the airflow improves heat dissipation and oxygen transport, but it also significantly increases the partial pressure gradient of water vapor and aggravates membrane dehydration [8]. In addition, ambient temperature, air humidity, and fan operating conditions can further amplify this coupling effect, making the performance and consistency of open-cathode air-cooled PEMFCs more sensitive to operating conditions [9,10]. Therefore, water management and thermal management remain key factors limiting the stable operation of air-cooled PEMFCs at high power density.

According to the above issues, extensive studies have been conducted from the perspectives of operational control, structural optimization, and enhanced thermal management. Ou et al. improved the output performance of open-cathode PEMFCs through coordinated regulation of temperature and humidity, demonstrating that external humidity and stack temperature control play a significant role in alleviating membrane dehydration [11]. Zeng et al. further experimentally revealed the mechanisms by which variable fan speed control affects stack temperature, single-cell voltage consistency, and parasitic power consumption [12]. In terms of stack thermal management, Chang et al. conducted in situ measurements of the internal temperature distribution in an open-cathode air-cooled stack and pointed out that airflow has a decisive influence on both the internal and external temperature difference of single cells and overall temperature uniformity [13]. From a control perspective, Yu et al. proposed a predictive control strategy that accounts for variations in ambient temperature, thereby achieving better stack temperature regulation and lower fan power consumption [14]. These studies have provided an important foundation for the thermal management of open-cathode PEMFCs, yet their focus has remained mainly on airflow regulation, flow field and structural design, or temperature control, while research on using the evaporation phase change of externally atomized droplets to simultaneously achieve rapid humidification and enhanced heat dissipation is still relatively limited.

On the other hand, numerical simulation has become an important tool for revealing the evolution of water and heat transport inside PEMFCs. Sagar et al. developed a computational model for open-cathode PEMFCs and analyzed the spatial variation characteristics of internal states such as relative humidity, temperature, and membrane water content [15]. Atyabi et al. further established a three-dimensional multiphase model of an open-cathode PEMFC to evaluate the effects of additional cooling channels on heat and mass transfer as well as polarization losses [16]. In addition, Yao reviewed the potential applications of ultrasound as an emerging technology in heating, ventilation, and air conditioning (HVAC), and pointed out that ultrasound can produce a variety of effects and is useful in applications involving heat or mass transfer by reducing external and internal transport resistance [17]. Navarro et al. employed an ultrasonic spray atomizer and established a three-dimensional multiphase flow numerical model, revealing the nonlinear influence of atomized droplet size distribution on evaporative cooling efficiency, identifying the optimal operating range for overall performance, and showing that a more uniform distribution of water mist throughout the controlled section is beneficial for a uniform and effective evaporative cooling process [18]. However, according to the existing representative studies, there is still limited work that introduces ultrasonically atomized droplets into open-cathode air-cooled PEMFCs and combines three-dimensional multiphysics modeling with stack experiments to systematically reveal the intrinsic relationships

 doi:10.20944/preprints202604.0542.v1

among droplet evaporation, local precooling, humidification in the active region, and temperature uniformity.

Distinct from previous studies, this work proposes a hydrothermal management strategy for air-cooled PEMFCs based on the coordinated control of ultrasonic atomization humidification and fan speed regulation, and conducts an in-depth investigation through a dual validation approach combining three-dimensional multiphysics simulation with stack experiments. On the one hand, by establishing a three-dimensional single-cell multiphysics model that incorporates electrochemical reactions, species transport, heat transfer, and droplet evaporation phase change, the mechanisms by which atomized droplets affect the temperature and humidity fields in the flow channels, the local potential distribution, and reaction uniformity are revealed. On the other hand, based on a 300 W open-cathode air-cooled PEMFC experimental platform, the polarization performance, single-cell voltage consistency, and infrared thermal response under different atomization frequencies, water temperatures, and fan speeds are validated, thereby enabling bidirectional regulation of membrane water content and stack temperature and improving the operating stability and response capability of air-cooled PEMFCs under medium and high-power conditions. The main innovations of this work are as follows:

(1) ultrasonic frequency modulation is used to actively regulate the humidification rate, effectively decoupling membrane hydration demand from the cooling airflow and thereby addressing the drying problem under high-load ventilation conditions;

(2) the microscale local potential and temperature gradients obtained from simulation are precisely correlated with the experimentally measured voltage consistency of 29 single cells and infrared thermography (IR) data, thereby revealing the mechanism for eliminating local hot spots;

(3) the Stokes number and Dalton's law of partial pressures are introduced to analyze, from a microscopic kinetic perspective, the physical mechanisms by which droplet agglomeration induces flooding and high-water vapor concentration dilutes the oxygen partial pressure.

By examining the effects of the coordinated control strategy of ultrasonic atomization humidification and fan speed regulation on stack output performance and the uniformity of thermal and humidity distribution, this study verifies its effectiveness in enhancing system output power, provides deeper insight into the evolution of multiphysics fields inside air-cooled stacks, and offers theoretical support for the stable operation of lightweight, high-power-density air-cooled PEMFC systems in complex environments.

2. Mathematical Model and Experimental Systems

2.1. Experimental Test Platform and Operating Condition Configuration

To validate the accuracy of the three-dimensional multiphysics model and provide reliable boundary conditions for the simulations, an integrated open-cathode air-cooled PEMFC experimental platform with a rated power of 300 W was established in this study, as shown in Figure 1. The stack consists of 29 single cells, each with an effective active area of 26 cm^2. The humidification module employs a customized ultrasonic atomization system with 12 microporous atomizing plates symmetrically arranged inside the inlet manifold. Through a multi-channel driver control board, the atomization frequency can be precisely adjusted within the range of 95 to 105 kHz. Meanwhile, the system is equipped with a thermostatic water bath to regulate the atomization water temperature, and the speed of the axial fan at the cathode outlet is linearly controlled by a PWM signal to achieve coordinated regulation of the hydrothermal distribution. Through experimental investigation, the optimal control parameters were explored to realize coordinated control of the vibration frequency of the atomizing plates and the fan speed, thereby regulating the humidity and cooling intensity of the air entering the stack, optimizing the internal water distribution and thermal management of the stack, and improving the overall system performance and stability.

 doi:10.20944/preprints202604.0542.v1

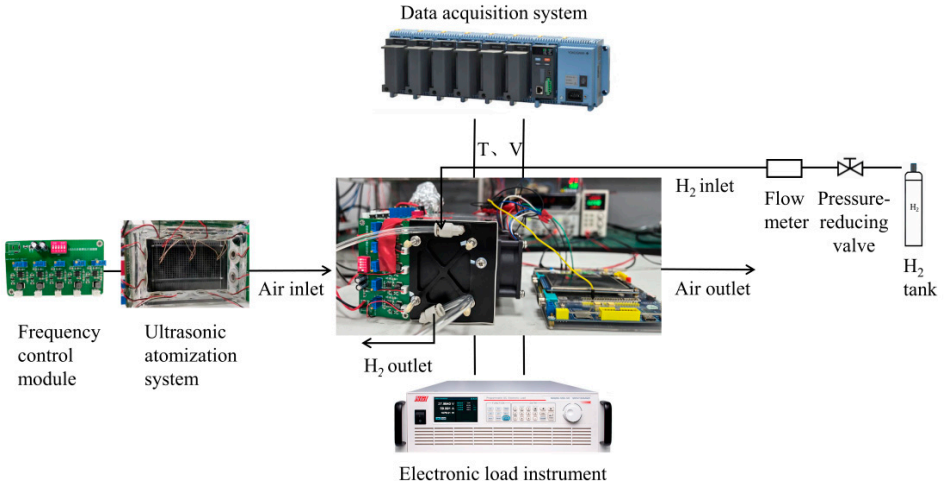

Figure 1. Integrated evaporative phase change cooling and humidification system for an air-cooled PEMFC.

2.2. Ultrasonic Atomization Humidification

In air-cooled PEMFC systems, cathode air serves not only as the oxidant for the electrochemical reaction but also as the cooling medium for removing waste heat. The essence of evaporative cooling lies in utilizing the large amount of latent heat absorbed when liquid water undergoes phase change into water vapor. Fine mist droplets are introduced into the stack flow channels through forced convection, where they rapidly evaporate and absorb heat in high-temperature regions, thereby effectively suppressing local overheating. Meanwhile, the water vapor generated by the phase change significantly increases the relative humidity (φ) of the air entering the reaction zone. Relative humidity is defined as the ratio of the partial pressure of water vapor in humid air (Pvapor) to the saturation vapor pressure (Ps) at the same temperature and pressure:

$$\varphi = \frac{P_{vapor}}{P_S} \quad (1)$$

When φ = 1, the air is considered to be at saturation. Appropriate humidification can reduce temperature while maintaining the relative humidity of the airflow at a high level, thereby preventing dehydration of the proton exchange membrane under forced convection.

Unlike conventional heated bubble humidification, ultrasonic atomization is based on the principle of piezoelectric transduction. When the piezoelectric ceramic on the surface of the atomizing plate is excited by a high-frequency alternating current, high-frequency acoustic standing waves are generated at the liquid interface, breaking the liquid surface tension and stripping the liquid into fine droplets to achieve atomization. Under stable atomization conditions, the initial diameter d of the droplets generated by the spray and the ultrasonic driving frequency f follow the classical Lang equation:

$$d = 0.34 \cdot \left(\frac{8\pi\sigma}{\rho f^2}\right)^{\frac{1}{3}} \quad (2)$$

Here, σ denotes the liquid surface tension, and ρ denotes the liquid density. Increasing the atomization frequency produces finer droplets. Fine droplets possess a very large specific surface area, which allows them to evaporate rapidly in the air channel and enter the stack uniformly with the airflow, making ultrasonic atomization particularly suitable for millisecond humidification response under dynamic PEMFC operating conditions.

The self-developed ultrasonic spray system used in the experiments is shown in Figure 2. To ensure uniform spray distribution, the system symmetrically arranged 12 microporous atomizing plates inside an acrylic manifold water tank. When water is forced into micropores with a diameter

 doi:10.20944/preprints202604.0542.v1

of approximately 4 to 5 μm, it is ejected in the form of droplet jets under high-frequency mechanical vibration. In the system-level measurements conducted in this study, the actual spray mass flow rate of the 12-plate module was 0.49 to 0.77 g/min at 95 to 105 kHz. To achieve precise control of the atomization frequency, a multi-channel driver control board based on the NE555 timer chip was developed, which generates square-wave signals by adjusting the external resistor-capacitor network (RC network).

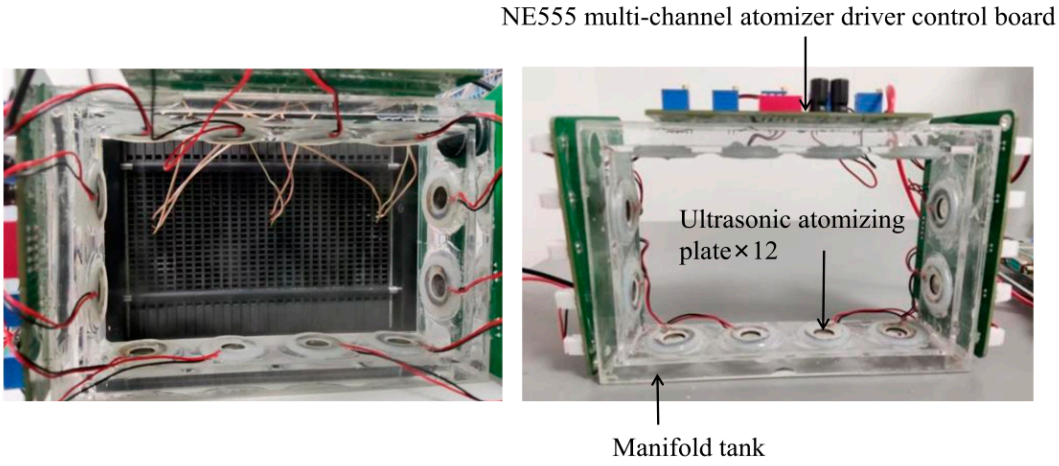

Figure 2. Ultrasonic Spray System.

2.3. Physical and Chemical Governing Equations

The interior of a fuel cell is a complex system involving strongly coupled gas, liquid, and solid multiphase flow and electrochemical reactions. To accurately reproduce in three-dimensional space the regulation mechanism of ultrasonic atomization humidification on the hydrothermal distribution within the stack, a non-isothermal single-cell multiphysics model was established in the COMSOL Multiphysics environment.

Fluid dynamics and heat transfer are mainly used to calculate how the cooling air flows through the cathode channels and how the reaction waste heat is removed during this convective process. The gas-phase flow and heat transfer behavior are governed by the continuity equation, the momentum conservation equation, and the energy conservation equation:

$$\nabla \cdot \left(\varepsilon \rho_g u_g\right) = S_{m,g} \tag{3}$$

$$\nabla \cdot \left(\varepsilon \rho_g u_g u_g\right) = -\varepsilon \nabla p_g + \nabla \cdot (\varepsilon \tau) + S_{mom} \tag{4}$$

$$\nabla \cdot \left(\varepsilon \rho_f c_p u T\right) = \nabla \cdot \left(k_{f,s}^{eff} \nabla T\right) + S_E \tag{5}$$

Here, the subscripts *g*, *f*, and *s* denote the gas phase, liquid phase, and solid phase, respectively; ε represents the porosity of porous media such as the gas diffusion layer (GDL) and is equal to 1 in the free flow channel; S denotes the source term. The viscous stress tensor τ is determined by the following equation:

$$\tau = \mu_g\left(\nabla u_g + \nabla u_g^T\right) - \frac{2}{3}\mu_g\left(\nabla \cdot u_g^T\right)I \tag{6}$$

The core process of a fuel cell is the generation of electricity through the electrochemical reaction between hydrogen and oxygen. The species transport and electrochemical reaction modules calculate the diffusion and consumption of hydrogen, oxygen, and water vapor in porous media, as well as the resulting current distribution. The species transport equation is given as follows:

 doi:10.20944/preprints202604.0542.v1

$$\nabla \cdot \left(\varepsilon \rho_g u_g \omega_i\right) + \nabla \cdot J = S_{m,i} \tag{7}$$

In the active region, the conservation of charge for protons and electrons is described by the following equations, respectively:

$$\nabla \cdot (\sigma_H \nabla \phi_H) + S_H = 0 \tag{8}$$

$$\nabla \cdot (\sigma_e \nabla \phi_e) + S_e = 0 \tag{9}$$

The electrochemical reaction rates at the anode and cathode differ significantly: the anode reaction is very fast and is described using a concentration dependent linear approximation, while the cathode exhibits slower kinetics and a higher overpotential, and its polarization behavior is described by Tafel kinetics:

$$j_a = a i_{0,ref}^{H_2} \left(\frac{c^{H_2}}{c_{ref}^{H_2}}\right)^{0.5} \frac{\alpha_a + \alpha_c}{RT} F\eta \tag{10}$$

$$j_c = -a i_{0,ref}^{O_2} \frac{c^{O_2}}{c_{ref}^{O_2}} \exp\left(-\frac{\alpha_c}{RT} F\eta\right) \tag{11}$$

After the micrometer sized droplets generated by ultrasonic atomization enter the high temperature flow channels, intense evaporation phase change occurs. This process substantially alters the local humidity distribution inside the flow channels, and the dynamic mass source term associated with the phase change between liquid water and water vapor is expressed as follows:

$$S_{g,l} = \begin{cases} \gamma_{l-g} \varepsilon s c \left(\frac{T}{343}\right)^{2.334} \frac{10^5}{p_g} \frac{M_{H_2O}}{RT} p_s \ln\left(\frac{p_s - p_{sat}}{p_s - p_v}\right), p_v \le p_{sat} \\ \gamma_{l-g} \varepsilon (1-s) c \left(\frac{T}{343}\right)^{2.334} \frac{10^5}{p_g} \frac{M_{H_2O}}{RT} p_s \ln\left(\frac{p_g - p_{sat}}{p_g - p_v}\right), p_v > p_{sat} \end{cases} \tag{12}$$

Meanwhile, the energy source term S_E accounts for all thermal interactions within the system, mainly including the Joule heat generated by electrochemical reactions ($S_{E,j}$), the phase change latent heat absorbed during the evaporation of ultrasonically atomized droplets ($S_{E,p}$), and the irreversible overpotential heat ($S_{E,irv}$):

$$S_{E,j} = \|j\|^2 / \sigma \tag{13}$$

$$S_{E,p} = S_{m,p} H_p \tag{14}$$

$$S_{E,irv,a} = j_a \left(|\eta_a| - \frac{T\lambda s_a}{2F}\right) \tag{15}$$

$$S_{E,irv,c} = j_c \left(|\eta_c| - \frac{T\lambda s_c}{4F}\right) \tag{16}$$

2.4. Model Geometry, Boundary Conditions, and Experimental Validation

To more precisely analyze the beneficial effects of ultrasonic atomization humidification on hydrothermal distribution and performance during PEM fuel cell operation, a three-dimensional multiphysics single-cell model of the PEM fuel cell was established in the COMSOL Multiphysics 6.4 environment, and the coupled processes of electrochemical reaction, charge and species transport, and heat transfer within the system were investigated in detail. The geometric configuration of the model is shown in Figure 3, in which orthogonal air flow channels on the cathode side and hydrogen flow channels on the anode side were constructed according to the experimental setup, with the cathode GDL, cathode catalyst layer (CL), proton exchange membrane (PEM), anode catalyst layer (CL), and anode GDL sequentially stacked between the flow channels.

 doi:10.20944/preprints202604.0542.v1

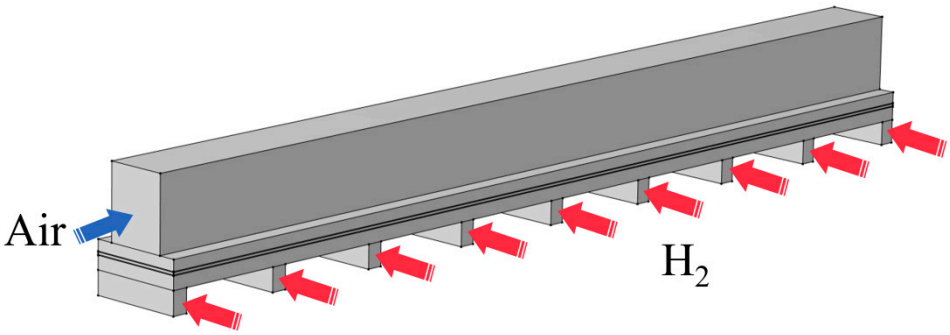

Figure 3. Three-dimensional multiphysics single-cell model.

To simulate the stacked cell configuration, periodic temperature boundary conditions were applied at the boundaries. The initial temperature of the model was set to 50 °C, and the inlet temperature of the oxygen phase was set to 55 °C. Meanwhile, different levels of surface convective heat transfer were defined at the other external boundaries of the model according to the actual physical packaging conditions of the stack. The cathode current collector boundary was set as electrical ground, while the anode was subjected to the corresponding constant current density according to different load conditions in the experiments, thereby driving the internal electrochemical reactions. To simulate the different behaviors under air cooling and ultrasonic atomization cooling conditions, different humidity values and thermal conductivities were assigned to the supplied air.

3. Results

3.1. Baseline Performance Analysis Under Conventional Air Cooling and Validation of the Multiphysics Model

As the core actuator for air supply and heat dissipation, fan speed governs the gas flow rate, convective heat transfer, and water evaporation within the flow channels, thereby directly regulating membrane hydration and stack performance. In the baseline polarization curve tests, to eliminate the influence of temperature fluctuations on performance, the fan speed (PWM duty cycle) was dynamically adjusted at each test point to stabilize the stack temperature strictly at the target operating temperature of 50 °C (±1 °C) before data acquisition, and the corresponding optimal fan speed at thermal equilibrium was recorded. Figure 4 shows the response characteristics of stack voltage, power, and optimal fan speed under different load conditions. As indicated by the polarization curve, with the gradual increase in current density, the average single-cell voltage exhibits a typical nonlinear decline that can be divided into three stages: in the low-load region of 0 to 0.2 A/cm², the voltage decreases slowly and is mainly dominated by activation polarization; in the medium-load region of 0.2 to 0.8 A/cm², ohmic loss becomes dominant, resulting in a more pronounced linear voltage drop; in the high-load region above 0.8 A/cm², the voltage declines sharply because of mass transport resistance and hydrothermal imbalance, showing a strong concentration polarization characteristic. The power curve shows that the output power of the fuel cell first increases and then decreases with increasing current density, with the maximum output power reaching 310.44 W at approximately 1.0 A/cm², which represents the optimal operating point of the system in this experiment. Beyond this point, although the current continues to increase, the voltage drops rapidly, causing the power to decrease instead, which indicates possible local membrane drying or hindered mass transport.

The optimal fan speed (PWM %) corresponding to each current density condition is the minimum stable airflow required for the stack to maintain the target operating temperature and membrane hydration state, representing the balance point between system safety and performance.

 doi:10.20944/preprints202604.0542.v1

Under low-load conditions (<0.2 A/cm²), the heat dissipation demand is weak, and the required fan speed remains low (12% to 20%). Upon entering the medium-load region, the airflow increases significantly from 20% to 86.5% in order to simultaneously satisfy the demands of heat dissipation and membrane hydration. In the high-load region (>0.8 A/cm²), the fan speed approaches saturation (99%), indicating that the system is nearing the physical limit of air cooling and must rely on maximum ventilation to suppress local overheating, although this inevitably accelerates water removal and increases the risk of membrane dehydration. The experimental results reveal the physical limitation of relying solely on fan speed regulation to balance heat dissipation and humidification.

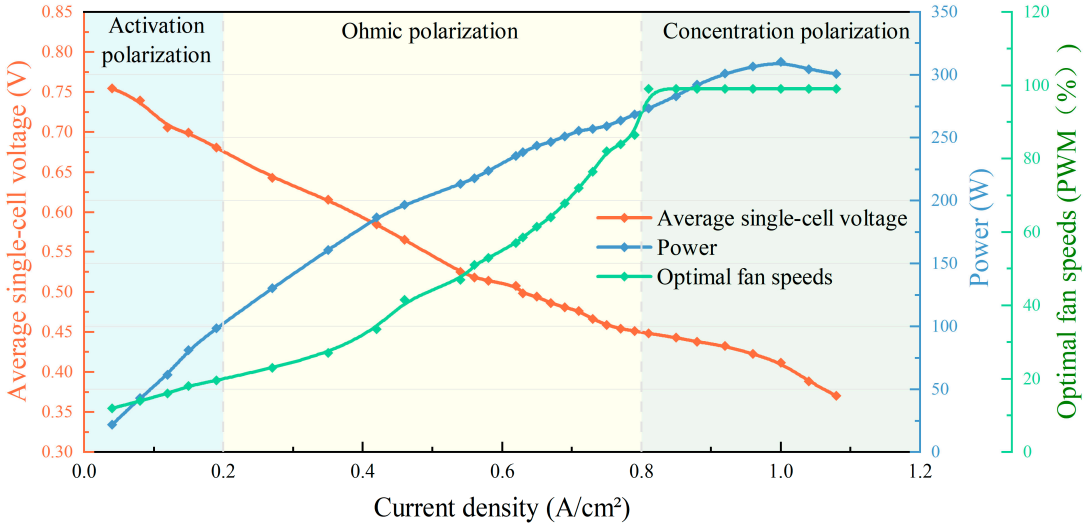

Figure 4. Polarization curve and power curve at the optimal fan speed.

To verify the reliability of the three-dimensional multiphysics model, reveal the hydrothermal evolution mechanism at the microscale, and evaluate the ultrasonic atomization strategy, steady-state simulations were conducted under actual experimental conditions using a combination of an ultrasonic vibration frequency of 100 kHz and a water temperature of 55 °C to validate the power performance of the model at different current densities. A comparison between the simulation results and the experimental data is shown in Figure 5. It can be seen that, under both conventional air cooling and atomization cooling conditions, the simulated polarization curves agree closely with the experimental measurements, and the very small errors over the entire current density range demonstrate that the model successfully and accurately captures the mass transport resistance, ohmic loss, and phase change thermal effects in the porous media. This three-dimensional multiphysics model can realistically reproduce the physicochemical processes inside the stack and provides a foundation for further in-depth analysis of the microscale hydrothermal evolution mechanism within the flow channels.

 doi:10.20944/preprints202604.0542.v1

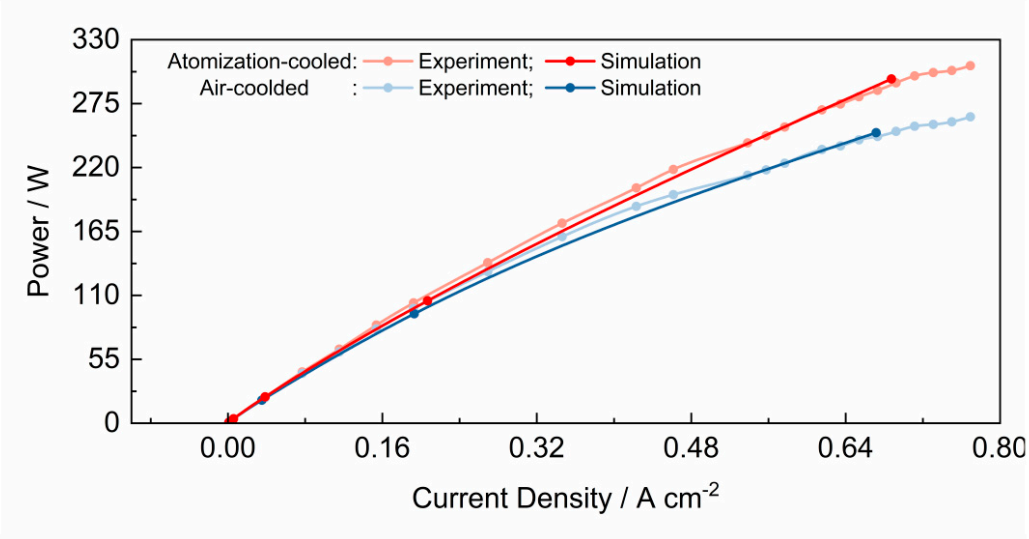

Figure 5. Experimental and simulated polarization curves under conventional air cooling and ultrasonic atomization cooling.

3.2. Enhancement of Output Performance by Atomization Humidification and Its Internal Multiphysics Characteristics

Proton conduction in PEMFCs mainly depends on the hydrated network structure within the membrane, while the membrane water content directly determines its proton conductivity. Ultrasonic atomization technology actively regulates droplet diameter, concentration, and evaporation phase change rate to reshape the temperature and humidity fields within the flow channels, thereby overcoming the power limitation of conventional air cooling. Proper control of the water temperature in the external humidifier is of great importance for maintaining membrane hydration, achieving hydrothermal balance, and preventing flooding or membrane drying.

Experimental results show that ultrasonic atomization parameters, including frequency and water temperature, have a decisive influence on stack output performance. Figure 6 presents the stack power characteristic curves at water temperatures of 45 to 60 °C under different ultrasonic vibration frequencies, namely 0 kHz without humidification, 95 kHz, 100 kHz, and 105 kHz. To eliminate the interference caused by differences in airflow rate, all test points were evaluated using the optimal cooling fan speed corresponding to 95 kHz.

From the overall evolution of the polarization characteristics, taking a water temperature of 55 °C as an example, the performance enhancement effect of atomization frequency on the stack becomes increasingly pronounced as the load increases. In the low load region, for example at 0.0769 A/cm^2, the system load is light, the heat generation of the stack is low, and the membrane has a relatively low hydration demand, so the humidification effect under different vibration frequencies has little influence on output performance. After 100 kHz atomization was introduced, the power increased only from 42.9 W to 45.68 W, corresponding to an improvement of 6.5%, indicating that humidification at this stage mainly serves to maintain the baseline humidity level. In the medium load region, for example at 0.6154 A/cm^2, system heat generation increases and the risk of membrane dehydration becomes more severe, so the influence of membrane hydration on performance is significantly strengthened and the regulating effect of humidification frequency becomes more sensitive. Atomization at 100 kHz exhibits excellent hydrothermal balancing capability, increasing the power from 235.52 W under non humidified conditions to 279.57 W, which corresponds to an improvement of 18.7%. When the vibration frequency is further increased to 105 kHz, the performance instead declines to 244.16 W, showing a performance deterioration caused by excessive

 doi:10.20944/preprints202604.0542.v1

humidification. In the high load region, for example at 0.7692 A/cm², the stack performance under conventional air-cooling decreases rapidly because of severe membrane dehydration and mass transport limitation. Atomization at 100 kHz successfully delays the onset of the polarization knee toward a higher current region and increases the peak power significantly from 263.60 W without humidification to 319.00 W, with an improvement of as much as 21.0%, indicating that appropriate humidification can markedly improve membrane hydration and reaction uniformity and thereby enhance electrochemical reaction efficiency. However, at a vibration frequency of 105 kHz, the output power decreases to 278.76 W, representing a drop of nearly 13% from the peak value. This further confirms that excessive humidification cannot continuously improve performance and may instead suppress system efficiency by causing local reaction nonuniformity or aggravated concentration polarization due to restricted gas diffusion and water film accumulation.

A comparison of the power variation at different temperatures shows that the system performance improves continuously with increasing water tank temperature within the range of 45 to 55 ℃, and reaches the overall optimum at 55 ℃ in particular. At this stage, a favorable balance is achieved between the evaporation efficiency of the atomized droplets and the water retention capability of the membrane, which promotes the synergistic enhancement of proton transport and reaction rate. However, when the water temperature rises to around 60 °C, the output power instead begins to decline. This phenomenon indicates that although a higher temperature helps enhance the electrode reaction rate and the ionic conductivity of the membrane, the excessively high saturated vapor pressure simultaneously induces a pronounced oxygen dilution effect, thereby leading to a decline in the overall system performance.

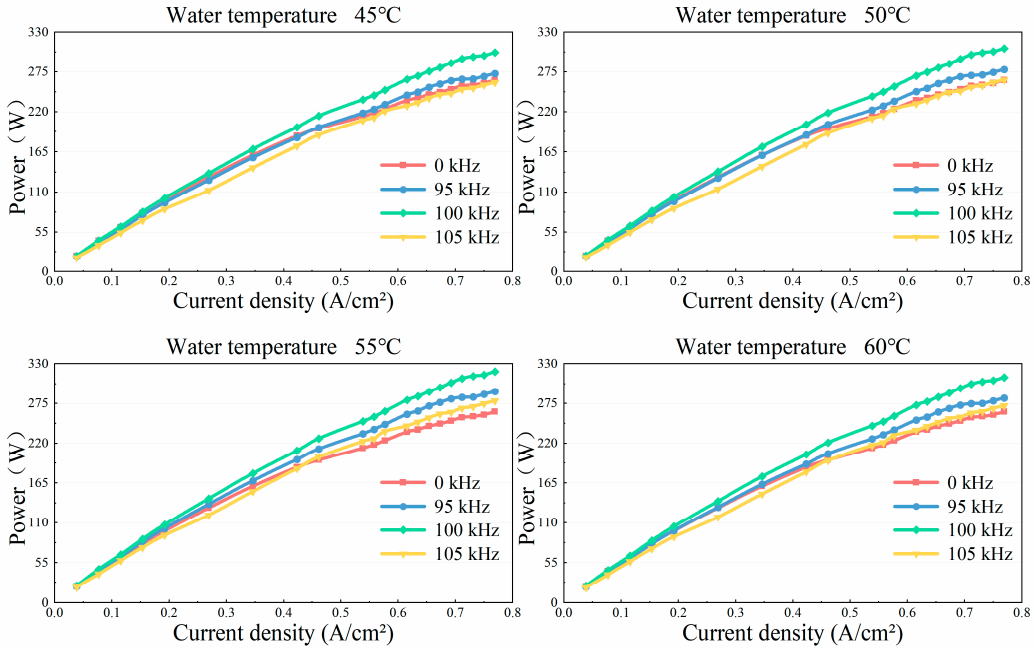

Figure 6. Variation of stack output power with current density under different water tank temperatures and ultrasonic vibration frequencies.

To elucidate the mechanism responsible for the performance enhancement under the optimal condition of 100 kHz and 55 °C, the developed COMSOL single-cell model was used to extract and analyze the internal three-dimensional hydrothermal distribution at ia = 0.038 A cm-2. Under the same cooling air velocity, conventional air cooling and ultrasonic atomization cooling exhibit fundamentally different thermophysical and mass transport characteristics.

The temperature and water mole fraction at the air inlet are shown in Figure 7a and Figure 7b. Under conventional air cooling conditions, because the system relies solely on the inflow of dry air, the inlet cross-section is affected by the backward conduction of reaction heat from inside the stack

 doi:10.20944/preprints202604.0542.v1

and exhibits an asymmetric high-temperature distribution, while the water mole fraction at the edge of the active region remains very low at only about 3%. After 100 kHz ultrasonic atomization is introduced, the dense micrometer-sized droplets begin to evaporate and absorb heat immediately upon contacting the high-temperature flow channels, causing the inlet cross-sectional temperature in Figure 7a to decrease significantly and become more uniform. Moreover, Figure 7b shows that the phase-change water vapor forms a highly concentrated enrichment layer, reaching more than 16%, in the region adjacent to the GDL. This efficient precooling and prehumidification at the inlet provide the basis for the subsequent heat and mass transfer processes throughout the entire flow channel.

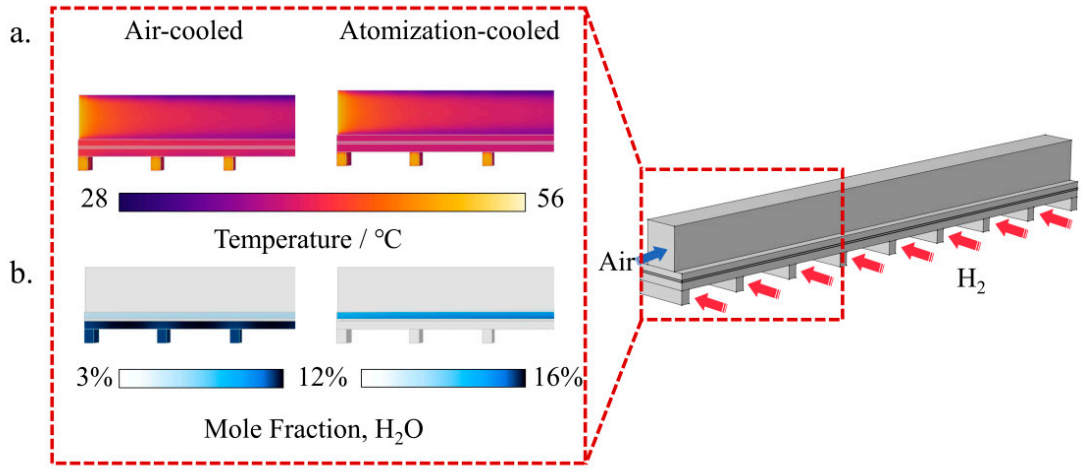

Figure 7. Comparison of inlet cross-sectional fields under conventional air cooling and ultrasonic atomization cooling: (a) temperature and (b) water mole fraction.

As the airflow progresses downstream, the temperature distribution in the active region at different positions along the air inlet direction and the heat flux distribution in the gas flow channels are shown in Figure 8a and Figure 8b. Conventional air cooling relies on sensible heat exchange through air, which leads to severe local heat accumulation and a large temperature gradient along the flow direction. In contrast, ultrasonic atomization cooling shifts the dominant mechanism from sensible heat exchange to latent heat absorption. The distributed evaporation of micrometer scale droplets within the flow channels produces a much gentler temperature gradient throughout the entire domain, fundamentally breaking the vicious cycle in which local hot spots lead to local membrane drying.

In air-cooled cells operating under high airflow cooling, the high-speed dry airflow creates a large water vapor concentration gradient between the membrane electrode and the flow channel, thereby forcibly removing water from the membrane. The distributions of water mole fraction and gas flow velocity are shown in Figure 8c and Figure 8d. It can be seen that the water vapor generated by phase change maintains a higher and more uniform water mole fraction in the active region of the membrane electrode, and this globally high hydration state preserves the proton conduction pathways in the PFSA ionomer network, ensures efficient proton transport, reduces local dehydration caused by forced convection, and greatly decreases the ohmic resistance to proton transport.

In summary, the three-dimensional multiphysics simulation results show that ultrasonic atomization is more than a simple physical humidification method, because it fundamentally improves the three-dimensional hydrothermal distribution within the flow channels through three microscopic physical mechanisms: rapid phase change precooling in the inlet region, latent heat absorption along the flow path, and effective water retention in the active region.

 doi:10.20944/preprints202604.0542.v1

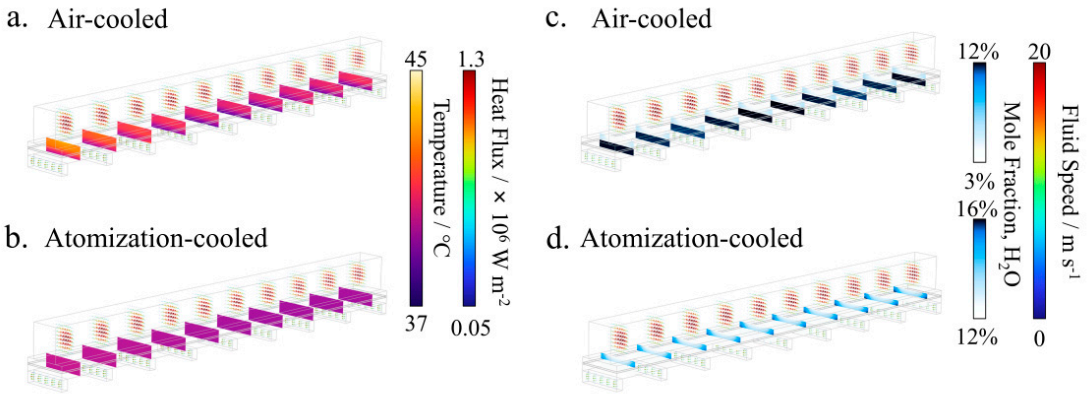

Figure 8. Comparison of temperature distribution in the active region and heat flux distribution in the gas flow channel: (a) conventional air cooling and (b) ultrasonic atomization cooling; comparison of water mole fraction distribution and gas velocity distribution: (c) conventional air cooling and (d) ultrasonic atomization cooling.

3.3. Evolution of Local Potential and Temperature Uniformity and Their Macroscopic Mapping

The nonuniformity of hydrothermal distribution inside PEMFCs not only limits the peak power of the system, but also serves as a major cause of accelerated material degradation in the membrane electrode assembly (MEA) and the onset of local thermal runaway. To verify the uniformity of the humidification module within the stack, a comparative analysis of the voltages of 29 single cells was conducted, and Figure 9 presents the single-cell voltage distributions before humidification (0 kHz) and after humidification (100 kHz) at different current densities.

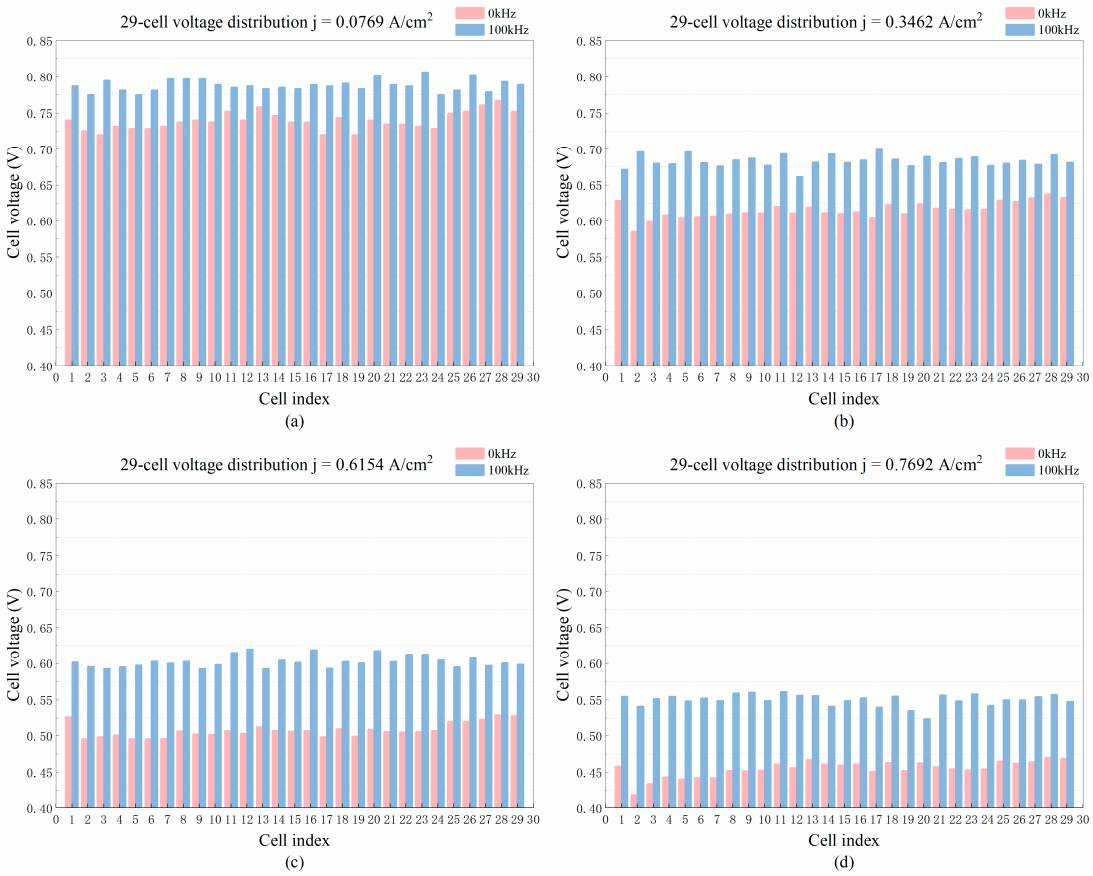

 doi:10.20944/preprints202604.0542.v1

Figure 9. Comparison of the voltage distributions of 29 PEMFC single cells at different current densities before humidification (0 kHz) and after humidification (100 kHz): (a) 0.0769, (b) 0.3462, (c) 0.6154, and (d) 0.7692 A/cm^2.

The results show that humidification not only improves the overall output level of the stack and increases the voltage, but also significantly enhances the uniformity within the stack. At j = 0.0769, 0.3462, 0.6154, and 0.7692 A/cm^2, the average single-cell voltage increased by approximately 48.8, 68.4, 94.9, and 95.5 mV, respectively, and the voltage increments of CH1 to CH29 were all positive at these four current densities, indicating that the performance improvement was not confined to a few cells but extended across the entire stack. In addition, the cell-to-cell dispersion decreased simultaneously, with the standard deviation reduced from 10.18 to 12.20 mV to 8.14 to 8.15 mV, and the range reduced from 34.2 to 52.3 mV to 27.3 to 38.1 mV (see Table 1). From the perspective of single-cell voltage consistency within the stack, these results indirectly confirm that atomization humidification provides more uniform membrane hydration and reaction conditions across the 29 cells.

Table 1. Statistical metrics of the voltages of 29 single cells at different current densities, including mean value, standard deviation, and range, comparing the conditions before humidification (0 kHz) and after humidification (100 kHz).

Current density j (A/cm^2)	Mean voltage (V), before / after	Standard deviation, SD (mV), before / after	Range (mV), before / after	Mean voltage increment, ΔMean (mV)
0.0769	0.7390 / 0.7878	12.20 / 8.15	47.2 / 31.5	48.8
0.3462	0.6152 / 0.6836	11.21 / 8.15	52.3 / 38.1	68.4
0.6154	0.5076 / 0.6025	10.18 / 8.14	34.2 / 27.3	94.9
0.7692	0.4545 / 0.5500	11.19 / 8.15	50.9 / 37.1	95.5

Figure 10 presents infrared (IR) thermal images of the stack inlet surface at four representative current densities, providing an intuitive visualization of the spatial temperature gradient and potential local hot spots. As shown in the figure, the reaction region of the stack appears as a continuous high-temperature plateau covering a relatively large area, with no abnormal local hot spots observed. Even under higher loads, the high-temperature region does not contract into localized hot spots. The maximum temperature difference mainly originates from the boundary heat-sink effect and manifests as a continuous gradient instead of isolated local hot spots. The experimental results indicate that the droplets disperse and evaporate over a wide area and achieve distributed heat dissipation through latent heat absorption and enhanced convective heat transfer, so the twelve-plate atomization cooling configuration can realize more uniform surface heat dissipation and effectively reduce the risk of local hot spots within the investigated operating range.

 doi:10.20944/preprints202604.0542.v1

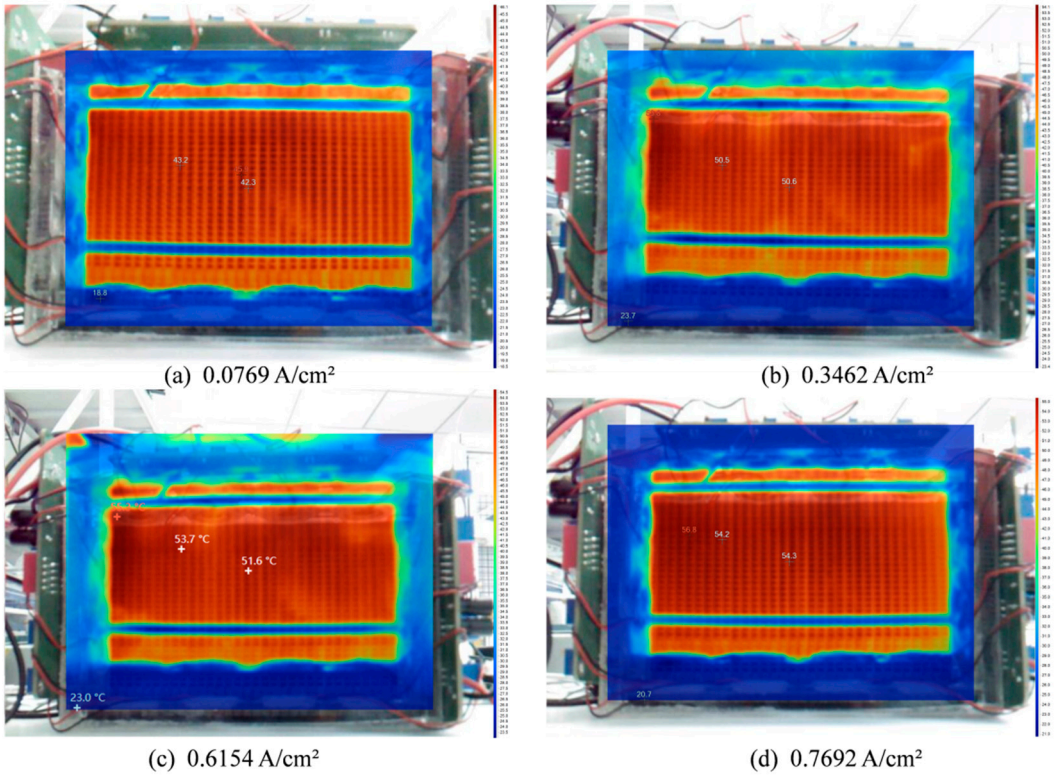

Figure 10. Infrared (IR) thermography of the stack inlet surface at representative current densities. The color bar indicates the surface temperature (°C).

To further investigate the effect of ultrasonic atomization cooling on model uniformity, two sampling lines were defined along the air inlet direction at the geometric centers of the anode and cathode GDL, and the distributions of voltage and temperature along these lines were analyzed at different current densities. As shown in Figure 11a and Figure 11b, under all load conditions, the local potential under conventional air-cooling exhibits pronounced fluctuations along the flow direction, mainly due to local membrane dehydration caused by forced convection, which in turn leads to a significant increase in ohmic polarization resistance. In contrast, the potential curve under ultrasonic atomization is smoother along the normalized depth, indicating that ultrasonic atomization humidification maintains a continuous and uniform proton conduction network throughout the entire flow domain and effectively reduces local fluctuations in charge transport. This local potential uniformity is consistent with the experimentally observed improvement in voltage consistency among the 29 single cells, and the stability of the charge transport pathways within the flow channels forms the basis for the highly consistent power output of the stack. As shown by the temperature sampling lines in Figure 11c and Figure 11d, conventional air cooling exhibits a pronounced temperature rise from the air inlet to the outlet. By comparison, the ultrasonic atomization case shows lower local temperatures and a flatter distribution, confirming that the continuous latent heat absorption associated with droplet phase change along the flow path effectively suppresses local temperature gradients. This flattened temperature profile is consistent with the IR thermography results, showing that ultrasonic atomization cooling enables the stack to form a large-area uniform temperature plateau, and that no isolated high-temperature peaks appear even under high load, which indicates that the atomized droplets achieve large-area uniform evaporative heat absorption within the flow channels and effectively suppress the risk of local overheating.

These results clearly demonstrate that ultrasonic atomization humidification enables large-scale uniform evaporative heat absorption within the flow channels, effectively eliminates high-temperature hot spots inside the stack, and alleviates local drying. This not only improves the peak output power of the system in the short term, but also fundamentally creates a mild and consistent

 doi:10.20944/preprints202604.0542.v1

operating environment for the membrane electrode assembly (MEA), thereby offering the potential to significantly suppress material degradation under high-load conditions and substantially extend the durability and reliability of the air-cooled stack.

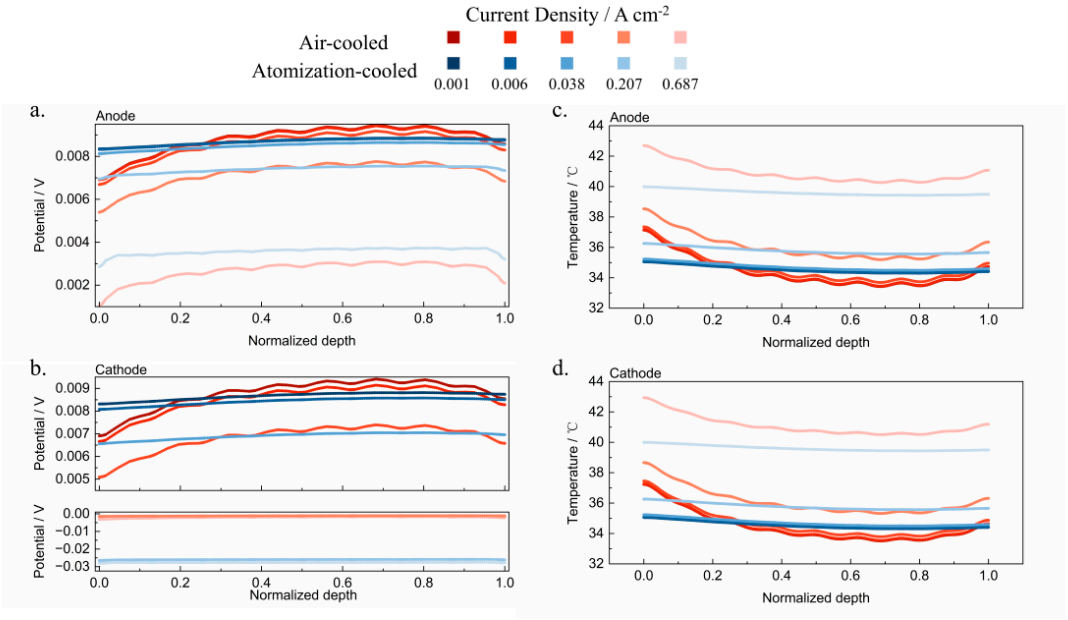

Figure 11. Comparison of local potential and temperature distributions along the sampling lines at the centers of the anode and cathode GDLs: (a) anode-side local potential, (b) cathode-side local potential, (c) anode-side temperature, and (d) cathode-side temperature.

3.4. Kinetic Boundaries of Microscopic Droplet Transport and Phase Change Mass Transfer

The preceding results show that stack performance does not increase monotonically with ultrasonic atomization frequency and water temperature, but instead reaches an optimum at 100 kHz and 55 °C. This nonlinear response originates from the coupled competition between droplet transport behavior and vapor-induced oxygen dilution inside the cathode channel. Therefore, the coordinated regulation strategy should be interpreted from both a fluid-dynamic and a mass-transfer perspective.

From the frequency perspective, increasing ultrasonic frequency reduces the initial droplet diameter according to the Lang relation, which favors evaporation by enlarging the specific surface area. However, the performance decline observed at 105 kHz indicates that single-droplet evaporation alone cannot explain the overall trend. The key factor is the behavior of the droplet swarm. To characterize droplet transport, the Stokes number is introduced as:

$$\mathrm{St} = \frac{\rho_p d^2 U}{18 \mu L_c} \tag{17}$$

where ρ_p denotes the droplet density (1000 kg/m^3), d the droplet diameter (m), U the characteristic airflow velocity (m/s), μ the dynamic viscosity of air (taken as 1.8 × 10^(-5) Pa·s), and Lc the characteristic length of the flow channel. At a frequency of 100 kHz, the generated droplets have a small diameter and a moderate number concentration, yielding $St \leq 1$, under which the droplets exhibit excellent flow-following behavior and can penetrate deeply into the reaction zone with the main gas stream. However, when the frequency increases to 105 kHz, the sharply increased droplet number concentration triggers intense Smoluchowski coagulation. Secondary coalescence causes a significant increase in droplet diameter d, and once a critical size is exceeded such that $St \geq 1$, the droplet motion shifts from drag-dominated behavior to inertia-dominated behavior. Because of inertia, large droplets deviate from the gas streamlines and directly impact and deposit on the surface of the gas diffusion layer (GDL), forming a continuous liquid film. At the microscopic level, this liquid

 doi:10.20944/preprints202604.0542.v1

film completely blocks the oxygen transport pathways, induces severe local flooding, and consequently leads to the macroscopic voltage decay observed in the output. Therefore, 100 kHz represents the kinetic critical threshold at which membrane hydration is maximized without inducing inertial deposition.

From the water-temperature perspective, increasing water temperature accelerates droplet evaporation and improves membrane hydration in the moderate range, which explains the performance enhancement from 45 to 55 °C. The evaporation characteristic time of a droplet can be expressed as:

$$\tau_{evap} = \frac{\rho_p d^2}{8\rho_g D_v \ln(1 + B_m)} \quad (18)$$

where ρ_g is the gas density, D_v is the diffusion coefficient of water vapor in air, and B_m is the Spalding mass transfer number. A higher water temperature reduces τ_{evap}, promoting faster phase change. However, when the water temperature is further increased to 60–65 °C, two adverse effects appear. First, a larger fraction of droplets evaporates prematurely before entering the region where in-channel evaporative cooling is most effective, thereby weakening latent-heat utilization inside the stack. Second, the increase in saturation vapor pressure raises the inlet water-vapor partial pressure and compresses the available oxygen partial-pressure space according to Dalton's law,

$$P_{O_2} = 0.21 \times (P_{total} - P_{H_2O}) \quad (19)$$

where P_{total} is the total inlet pressure, and P_{H2O} is the saturation vapor pressure at the corresponding water temperature.

Experimental results show that an excessively high-water temperature causes the saturation vapor pressure of water vapor in the inlet gas to increase exponentially, which inevitably and substantially reduces the available partial pressure space for oxygen. According to Fick's first law, a sharp decrease in oxygen partial pressure directly weakens the concentration gradient driving force for oxygen diffusion from the GDL side to the catalyst layer (CL), leading to severe concentration polarization under high-load conditions.

Overall, the optimal condition of 100 kHz and 55 °C can be understood as a coupled kinetic boundary. At this condition, droplet transportability, evaporation efficiency, latent heat utilization, and oxygen availability reach a favorable balance, which explains the simultaneous improvement in output performance, hydrothermal uniformity, and high load stability.

4. Conclusions

This study addresses the strong hydrothermal coupling problem encountered by open-cathode air-cooled PEMFCs under medium and high-power density operating conditions and proposes a hydrothermal management strategy based on the coordinated control of ultrasonic atomization humidification and fan speed regulation. By constructing a three-dimensional multiphysics single-cell model and combining it with a 300 W experimental platform, the mechanism underlying the performance enhancement was systematically investigated. The main conclusions are as follows:

(1) Active regulation of water mist through ultrasonic frequency adjustment can effectively alleviate the coupling conflict between membrane hydration demand and cooling airflow. Under the optimal coordinated condition of a 100 kHz atomization frequency and a water temperature of 55 °C, the stack significantly suppressed membrane dehydration induced by forced convection, and the peak power increased by 21.0% to 319.00 W.

(2) The three-dimensional multiphysics simulations show that ultrasonic atomization changes the conventional single hydrothermal management pathway of air-cooled PEMFCs. The rapid evaporation of micrometer-sized droplets within the flow channels not only effectively mitigated local hot spots, but also increased the water vapor content through phase change mass transfer and maintained a high and uniform water mole fraction distribution, thereby reducing proton transport resistance and improving reaction uniformity.

 doi:10.20944/preprints202604.0542.v1

(3) The one-dimensional sampling line results show that ultrasonic atomization makes the local potential and temperature distributions at the center of the GDL more uniform. This microscale uniformity is consistent with the experimental results and can explain the substantial convergence of the voltage dispersion among the 29 single cells, with the range decreasing by about 30% and the standard deviation dropping to 8.14 mV, as well as the intrinsic mechanism underlying the formation of a large-area uniform temperature plateau in IR thermography, indicating that this strategy helps reduce local overheating and the resulting risk of material degradation.

(4) The results show that the hydrothermal coordinated regulation process is simultaneously constrained by both fluid dynamic and thermodynamic mechanisms. Combined analysis based on the Stokes number and Dalton's law of partial pressures shows that an excessively high atomization frequency enhances the tendency of droplet agglomeration, leading to inertial deposition and inducing local flooding. When the water temperature rises to around 60 °C, the excessively high-water vapor partial pressure reduces the available oxygen partial pressure, weakens the driving force for oxygen mass transfer, and aggravates concentration polarization. Therefore, the parameter combination of 100 kHz and 55 °C achieves a favorable balance between preventing flooding and suppressing oxygen dilution.

In summary, the coordinated control strategy of ultrasonic atomization humidification and fan speed regulation can effectively alleviate the hydrothermal coupling conflict in open-cathode air-cooled PEMFCs under medium and high-power operation, significantly improve output performance, temperature uniformity, and cell-to-cell consistency, and show strong potential for suppressing local overheating and delaying membrane electrode degradation. This study provides a new perspective and technical support for optimizing hydrothermal management and enabling high power density operation of air-cooled PEMFCs, and demonstrates promising engineering applicability in weight-sensitive application scenarios such as unmanned aerial vehicles and portable power generation devices.

Although this study has verified the effectiveness of the coordinated control strategy of ultrasonic atomization humidification and fan speed regulation in the hydrothermal management of open-cathode air-cooled PEMFCs, several limitations still remain, and future work will focus on integrating dedicated exhaust condensation and water recovery modules to achieve closed-loop water balance. In addition, extension to higher-power systems will require further optimization of droplet transport characteristics, together with long-term durability cycling tests to verify reliability over the full lifecycle.

Author Contributions: J.Q.: Conceptualization, Methodology, Investigation, Formal Analysis, Data Curation, Visualization, Writing—Original Draft; H.M.: Conceptualization, Methodology, Software, Validation, Formal Analysis, Visualization; X.H.: Methodology, Investigation, Data Curation, Validation, Writing—Review and Editing; H.Y.: Methodology, Investigation, Visualization, Validation.

Data Availability Statement: The original contributions presented in this study are included in the article. Further data supporting the findings of this work are available from the corresponding author upon reasonable request.

Conflicts of Interest: The authors declare no conflicts of interest.

Abbreviations

The following abbreviations are used in this manuscript:

PEMFC	Proton exchange membrane fuel cell
PFSA	Perfluorosulfonic acid
MEA	Membrane electrode assembly
GDL	Gas diffusion layer
CL	Catalyst layer
IR	Infrared

 doi:10.20944/preprints202604.0542.v1

PWM Pulse-width modulation

References

1. Chang, Y.; Qin, Y.; Yin, Y.; Zhang, J.; Li, X. Humidification strategy for polymer electrolyte membrane fuel cells – A review. Applied Energy 2018, 230, 643-662, https://doi.org/10.1016/j.apenergy.2018.08.125.
2. Kandidayeni, M.; Macias, A.; Boulon, L.; Kelouwani, S. Investigating the impact of ageing and thermal management of a fuel cell system on energy management strategies. Applied Energy 2020, 274, 115293, https://doi.org/10.1016/j.apenergy.2020.115293.
3. Wang, Y.; Chen, K.S.; Mishler, J.; Cho, S.C.; Adroher, X.C. A review of polymer electrolyte membrane fuel cells: Technology, applications, and needs on fundamental research. Applied Energy 2011, 88, 981-1007, https://doi.org/10.1016/j.apenergy.2010.09.030.
4. Chen, J.; Sun, L.; Zhu, W.; Pei, H.; Xing, L.; Tu, Z. Influence of cathode air supply mode on the performance of an open cathode air-cooled proton exchange membrane fuel cell stack. Applied Thermal Engineering 2024, 243, 122709, https://doi.org/10.1016/j.applthermaleng.2024.122709.
5. Wang, L.; Quan, Z.; Zhao, Y.; Yang, M.; Zhang, J. Experimental investigation on thermal management of proton exchange membrane fuel cell stack using micro heat pipe array. Applied Thermal Engineering 2022, 214, 118831, https://doi.org/10.1016/j.applthermaleng.2022.118831.
6. Jiao, K.; Li, X. Water transport in polymer electrolyte membrane fuel cells. Progress in Energy and Combustion Science 2011, 37, 221-291, https://doi.org/10.1016/j.pecs.2010.06.002.
7. Chen, Q.; Zhang, G.; Zhang, X.; Sun, C.; Jiao, K.; Wang, Y. Thermal management of polymer electrolyte membrane fuel cells: A review of cooling methods, material properties, and durability. Applied Energy 2021, 286, 116496, https://doi.org/10.1016/j.apenergy.2021.116496.
8. Chen, Y.; Jian, Q.; Huang, Z.; Zhao, J.; Bai, X.; Li, D. Improvement of thermal management of proton exchange membrane fuel cell stack used for portable devices by integrating the ultrathin vapor chamber. International Journal of Hydrogen Energy 2021, 46, 36995-37006, https://doi.org/10.1016/j.ijhydene.2021.08.185.
9. Zhao, C.; Wang, F.; Wu, X. Analysis and review on air-cooled open cathode proton exchange membrane fuel cells: Bibliometric, environmental adaptation and prospect. Renewable and Sustainable Energy Reviews 2024, 197, 114408, https://doi.org/10.1016/j.rser.2024.114408.
10. Yang, Y.; Jia, H.; Liu, Z.; Bai, N.; Zhang, X.; Cao, T.; Zhang, J.; Zhao, P.; He, X. Overall and local effects of operating parameters on water management and performance of open-cathode PEM fuel cells. Applied Energy 2022, 315, 118978, https://doi.org/10.1016/j.apenergy.2022.118978.
11. Ou, K.; Yuan, W.-W.; Choi, M.; Yang, S.; Kim, Y.-B. Performance increase for an open-cathode PEM fuel cell with humidity and temperature control. International Journal of Hydrogen Energy 2017, 42, 29852-29862, https://doi.org/10.1016/j.ijhydene.2017.10.087.
12. Zeng, T.; Zhang, C.; Huang, Z.; Li, M.; Chan, S.H.; Li, Q.; Wu, X. Experimental investigation on the mechanism of variable fan speed control in Open cathode PEM fuel cell. International Journal of Hydrogen Energy 2019, 44, 24017-24027, https://doi.org/10.1016/j.ijhydene.2019.07.119.
13. Chang, H.; Cai, F.; Yu, X.; Duan, C.; Chan, S.H.; Tu, Z. Experimental study on the thermal management of an open-cathode air-cooled proton exchange membrane fuel cell stack with ultra-thin metal bipolar plates. Energy 2023, 263, 125724, https://doi.org/10.1016/j.energy.2022.125724.
14. Yu, X.; Zhang, C.; Li, M.; Wang, G.; Tu, Z.; Yu, T.; Dong, H.; Zhao, F. Thermal management of an open-cathode PEMFC based on constraint generalized predictive control and optimized strategy. Renewable Energy 2024, 220, 119608, https://doi.org/10.1016/j.renene.2023.119608.
15. Sagar, A.; Chugh, S.; Sonkar, K.; Sharma, A.; Kjeang, E. A computational analysis on the operational behaviour of open-cathode polymer electrolyte membrane fuel cells. International Journal of Hydrogen Energy 2020, 45, 34125-34138, https://doi.org/10.1016/j.ijhydene.2020.09.133.
16. Atyabi, S.A.; Afshari, E.; Shakarami, N. Three-dimensional multiphase modeling of the performance of an open-cathode PEM fuel cell with additional cooling channels. Energy 2023, 263, 125507, https://doi.org/10.1016/j.energy.2022.125507.

 doi:10.20944/preprints202604.0542.v1

17. Yao, Y. Research and applications of ultrasound in HVAC field: A review. Renewable and Sustainable Energy Reviews 2016, 58, 52-68, https://doi.org/10.1016/j.rser.2015.12.222.
18. Navarro, P.; Ruiz, J.; Martínez, P.; Lucas, M. Numerical study of an ultrasonic spray atomiser as an evaporative cooler. Applied Thermal Engineering 2024, 236, 121455, https://doi.org/10.1016/j.applthermaleng.2023.121455.